# Effects of in-cylinder non-uniformities on mixture preparation in a light-duty Diesel engine operating a light-load Partially Premixed Combustion strategy

F. Perini[1], K. Zha[2], D. Sahoo[2], S. Busch[2], P. C. Miles[2], R. D. Reitz[1]

[1]Engine Research Center, University of Wisconsin-Madison. Madison, WI, USA.

E-mail: perini@wisc.edu, reitz@engr.wisc.edu
Telephone: +(1) 608-263-2735

[2]Combustion Research Facility, Sandia National Laboratories. Livermore, CA, USA.

E-mail: kzha@sandia.gov, sbusch@sandia.gov, pcmiles@sandia.gov
Telephone: +(1) 925-294-1512

**Abstract.** The emissions, performance, and control of advanced combustion strategies such as Partially Premixed Combustion (PPC) is strongly affected by local fuel-air mixture preparation. In this work, we combine computational and experimental approaches to study the effects of combustion chamber geometric details and intake-induced non-uniformities in the temperature and velocity fields on the operation of a single cylinder, light-duty diesel engine operating in a slightly boosted, light-load partially-premixed compression ignition (PPCI) mode. A comprehensive computational model of the single-cylinder research engine was developed considering the complete intake and exhaust ducts and the plenums' geometries, as well as adjustable throttling devices used to obtain different swirl ratios. The in-cylinder flow predictions were validated against PIV measurements at different swirl ratio configurations, confirming the reliability of the RANS turbulence modeling approach in capturing ensemble-averaged flow field properties. A batch of multidimensional simulations was then set up to model corresponding mixture preparation experiments, faturing a non-reactive charge and a single, early injection pulse, under different swirl ratio and injection pressure conditions. Finally, the effects of geometric details on velocity field non-uniformity were studied, showing that, even if it is not possible to simulate differences arising from deposits or injector nozzle-by-nozzle non-uniformities, detailed multidimensional modeling can noticeably improve the predictability of local mixture quantities that affect ignition and pollutant formation.

## 1. Introduction

The success of advanced, fuel-efficient and environmentally sustainable combustion strategies such as reactivity-controlled compression ignition (RCCI), homogeneous-charge compression ignition (HCCI), partially-premixed compression ignition (PPCI), and gasoline direct-injection compression ignition (GDICI) will be determined by the possibility to control combustion development locally, in-cylinder. Much of the understanding developed by the study of these combustion modes has been made possible by advances in computer modeling, which in the last decade has allowed the incorporation of detailed chemistry calculations in engine CFD simulations [22]. The availability of detailed chemistry enabled accurate predictions of local ignition and in-cylinder pollutant emission sources, in simulations that already provided reasonably accurate estimates of the effect of phenomena such as wall boundary layers and of spray-turbulence interactions on mixture ignition and extinction.

However, comprehensive combustion calculations in realistic engine geometries need extensive computational resources, and predicted spray development typically shows significant mesh dependency. Thus, in the engine design phase, a sector mesh approach is still usually employed, where only one axisymmetric slice of the combustion chamber is modeled, assuming that both geometric and flow symmetries occur.

In this work, we implement and employ advanced, mesh-independent spray models in the Engine Research Center unstructured KIVA (KIVA-ERC) CFD solver for internal combustion engine

calculations, to study the effects of in-cylinder geometric and flow non-uniformities on mixture preparation in the Sandia National Laboratories (SNL) light-duty optical Diesel engine facility. Particle Image Velocimetry (PIV) of the flow field during intake and Planar Laser Induced Fluorescence (PLIF) of fuel tracer measurements were used to assess and compare the accuracy of the computational models in predicting local flow and compositional non-uniformities when using either a sector mesh or the full engine geometry representation.

## 2. Experimental Setup

All of the experiments were run in the Sandia National Laboratories optical Diesel engine facility. The experimental setup features a single cylinder engine, modified from a production GM 1.9L light-duty engine [6,8,18,20,23-24]. A schematic of the experimental configuration is reported in Figure 1. The engine features optical access through fused silica windows located at the top of the cylinder liner, as well as a fused silica piston which retains the full geometric details of the production piston. The only differences consist of a wider and deeper crevice region, which was designed to allow imaging within the piston bowl, and which slightly reduces the engine's effective compression ratio. The engine is equipped with a second-generation, 7-hole Bosch common-rail CRI2.2 fuel injector. The swirl ratio of the in-cylinder flow can be arbitrarily adjusted through throttle plates which are fitted in each of the intake ports, allowing for effective swirl ratios ranging from about Rs = 1.5 up to about Rs = 5.5. A summary of the engine's main geometric parameters and the operating conditions used for this study are reported in Table 1.

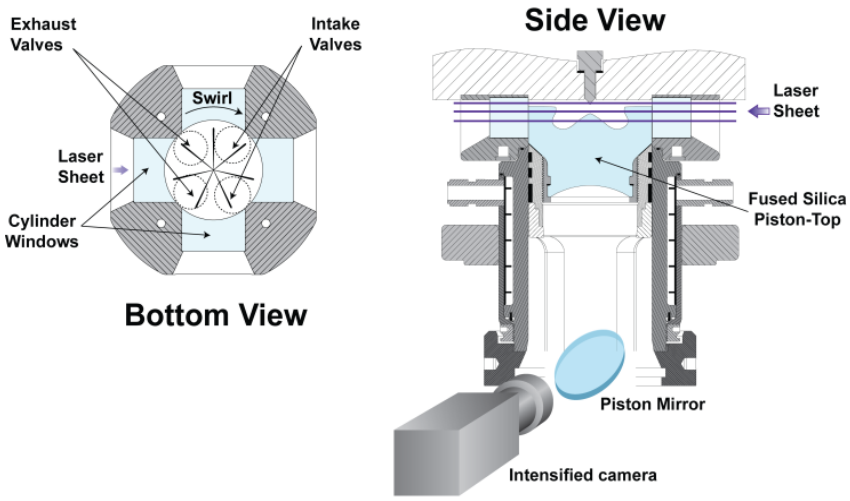


**Fig. 1.** Optical engine setup, including the three laser sheet locations and camera viewing direction.

Mixture preparation data for a non-reacting operating condition were obtained by planar laser-induced fluorescence (PLIF) [24,20]. Toluene was added as a fuel tracer to a PRF25 binary fuel mixture made of 25% iso-octane and 75% n-heptane. In order to realize non-reacting conditions, the engine was fed with a pure nitrogen charge. The nitrogen mass flow and intake temperature were calibrated in order to match the same near-TDC density and temperature of the corresponding operating condition with a reacting charge [24]. Ensemble averaged PLIF images of in-cylinder equivalence ratios were taken at four different swirl ratios: Rs = 1.5, 2.2, 3.5, 4.5, and at three horizontal planes within the combustion chamber: one (P1) located halfway within the squish region; one (P2) located at the bowl rim height, and a third one (P3) located deep within the piston bowl, at the height where it has its maximum radial extension. The plane positions varied due to changing piston position at every measurement timing, typically every 2.5 crank angle degrees from the start-of-injection and until TDC.

PIV measurements of flow patterns during the intake and compression strokes [28,29] were taken using borosilicate glass particles with 2 μm diameter, every 15 crank angle degrees during the intake and compression strokes. Measurements were taken at three horizontal planes located at fixed distances from the fire-deck, namely dz = 10.0, 13.5 and 17.0 mm.

**Table 1**. Engine and Experimental Setup details

| **Engine specifications** | |
|---|---|
| Bore x stroke [mm] | 82.0 x 90.4 |
| Unit displacement [$cm^3$] | 477.2 |
| Compression ratio | 16.4 : 1 |
| Squish height at TDC [mm] | 0.88 |
| **Bosch CRI2.2 Injector parameters** | |
| Number of holes | 7 |
| Included angle [deg] | 149 |
| Nozzle diameter [mm] | 0.14 |
| **Fuel properties for mixture preparation studies** | |
| Composition [mole fractions] | 75% $nC_7H_{16}$ |
| | 25% $iC_8H_{18}$ |
| Fluorescent tracer [mass fr.] | 0.5% $C_7H_8$ |
| Equivalent Cetane Number [-] | 47 |
| **Operating conditions** | |
| Intake charge composition | 100% $N_2$ |
| Intake pressure [bar] | 1.5 |
| Intake temperature [K] | 300.0 |
| Engine speed [rpm] | 1500 |
| Injected fuel mass [g] | 0.0088 |
| Start of injection [deg aTDC] | -23.3 |
| Rail pressure [bar] | 860 |
| Swirl ratio [-] | 1.5, 2.2, 3.5, 4.5 |

## 3. Computational Setup

Two computational models, employing either a sector mesh featuring one seventh of the combustion chamber, as adopted in previous studies [7,14,17], or a full engine geometry, including the intake and exhaust ports and pressure-damping vessels as used in the experiments [16], were built. Both models were run using a new, unstructured implementation of the KIVA-ERC code, similar to the finite volume KIVA-4 code [25].

### 3.1 Spray model implementation

The code was extensively bug-fixed and many computational efficiency improvements were introduced to handle large grids and large numbers of species efficiently.

The ERC-developed spray models were implemented, with a focus on computational efficiency and on the possibility to handle unstructured grids. The spray models included the hybrid Kelvin-Helmholtz/Rayleigh-Taylor breakup model, with Levich's breakup distance concept [3]; the unsteady gas-jet theory model for velocity field estimation in the under-resolved near-nozzle region [1]; a grid-independent collision model featuring deterministic collision parameter estimation and extended collision outcomes [12]; and a computationally improved version of the discrete multi-component vaporization model by Torres *et al*. [26]. A similar spray model setup has been shown to provide almost grid-independent prediction of spray drop sizes and jet penetration histories [27].

This model setup was improved by the introduction of dynamic parcel storage allocation to reduce the number of spray model parameters. In the new configuration, the 'blob' injection model [25], which models the initial liquid jet core as a train of 'blobs', with diameter equal to the effective orifice diameter, injects the exact number of blobs such that each computational parcel only includes one blob. Note that, after breakup occurs, a computational parcel typically tracks the behavior of an equivalent cloud of spray drops, which size distribution is modeled in terms of an equivalent Sauter Mean Radius (SMR). Then during runtime, as parcels undergo breakup, collisions, and vaporization,

and thus increase in number, the parcel storage size is updated based on the current requirements. The standard KIVA approach requires the user to specify a desired (and typically not large) number of parcels, which each contains more than one blob, introducing a further source of under-resolution in the spray.

Finally, the fuel drop drag model was improved by introducing a more accurate and fully analytical formulation of a sphere's drag coefficient [11], suitable for Reynolds numbers up to $Re = 2 \cdot 10^6$, which features all surface boundary layer regimes. The model was also extended with a Mach number effect estimation through a multiplier which is computed efficiently as a function of the Mach and Reynolds numbers [2] using Bezier interpolation. In the simulations, the RNG k-epsilon turbulence model [10] was used, while thermo-chemistry properties were evaluated using the SpeedCHEM chemistry solver [15] and the ERC reaction mechanism for Primary Reference Fuels (PRF) [21].

### 3.2 Engine model

Both the sector and full engine computational grids have been validated in previous studies: the sector mesh [7,14] for partially-premixed compression ignition (PPCI) and pilot injection mixture preparation [17], and the full mesh [16] for PIV flow measurement experiments [19], respectively. Both grids feature an average cell resolution of 0.7 mm in the combustion chamber near TDC, which leads to a total of 92850 and of 682091 cells at BDC, respectively.

A representation of the cross-sectional discretization for both grids is reported in Figure 2. The simplified geometry allowed the sector discretization to be extremely smooth, and the cell layers to be axisymmetrically rotated, while in the full geometry a body-fitted approach was employed. Also, Figure 2 shows how the effective squish height at TDC used in the sector mesh can deviate significantly from the actual, local squish height due to the non-even piston squish surface, which includes valve cut-outs, and due to the presence of a non-negligible volume fraction within the valve recesses. All of these factors deteriorate the sector model's accuracy in capturing the amount of flow being directed towards the interior of the combustion chamber from the squish region, as the piston approaches TDC.

The full mesh retains all piston and head geometric details, including valve cut-outs on the piston surface, valve recesses on the head, as well as the correct crevice size for the optical piston, which is slightly thicker and significantly deeper than the corresponding metal production piston [6]. Wide usage was made of O-grid structures: these are blocking structures useful to correctly discretize near-wall regions in circular shapes, where the kernel of the circular structure is occupied by a square block, and four other blocks are connected to each of its edges, filling the space up to the circular shape, and being inter-connected at 45-degree diagonals. O-grid structures were used to match all round and cylindrical shapes in the domain, including liner, valves, seats, ports, and piston bowl, to avoid badly skewed cells at all the relevant wall surfaces and thus achieve optimal wall boundary modelling. Specific attention was devoted to modelling the squish region, enclosed between the cylinder head and a virtual surface representing the piston crown when at TDC. In this region, a total of 10 cell layers was used, to achieve the same resolution as in the sector mesh, and to guarantee appropriate resolution of the flow structures during valve movement. The same layer thickness was used for the valves and valve seats, where eight more layers were used.

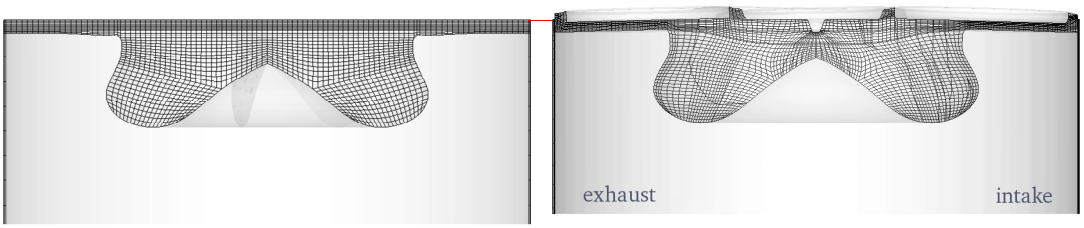


**Fig. 2.** Comparison between sector (left) and full engine mesh (right) at TDC

The same O-grid approach used for the valves was also applied to the injector protrusion region, which could thus be introduced in the engine model (shaped according to the injector drawings and a measured protrusion value of 1.85 mm). In this way, the near-nozzle region could be modelled using a homogeneous and axisymmetric discretization, meant to reduce, if not completely avoid, mesh dependency effects on predicted jet-to-jet differences in the spray simulation.

Also, the computational domain for the full engine mesh, which already included both intake and exhaust ports, was improved by incorporating the pressure damping vessels at the outlets, as reported in Figure 3. Thanks to the availability of time-resolved intake and in-cylinder pressure measurements, all flow and mixture preparation studies were initialized at exhaust valve opening (EVO), so that the simulation of the complete exhaust and intake strokes allowed proper flow and turbulence development.

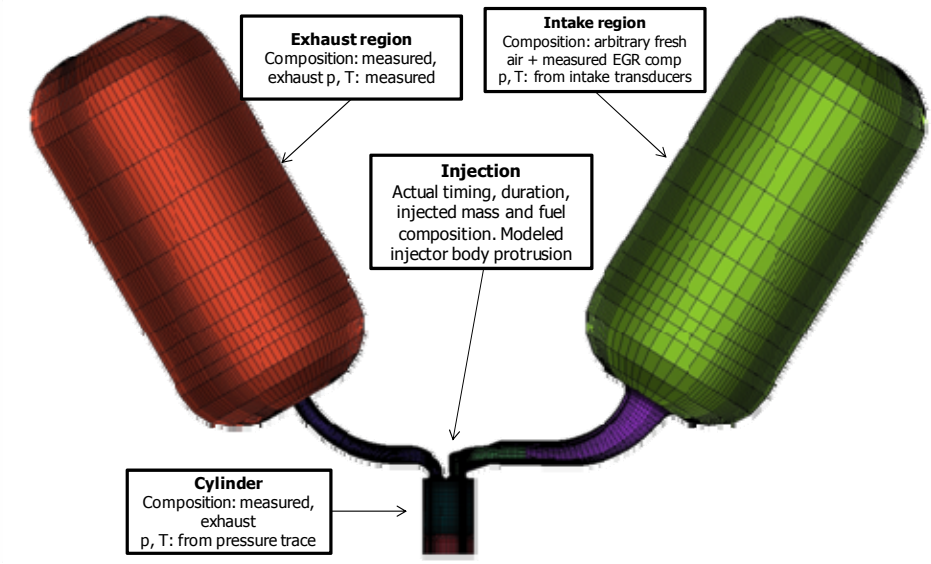


**Fig. 3.** Overview of the full engine geometry simulation setup

### 3.3 Swirl generation modeling

The optical engine in this study features a swirl control device (Figure 4) placed immediately upstream of the in-head portions of the intake ports, and downstream of the intake runners [13]. This device contains two ducts having the same cross-sectional shape as the intake ducts, where two throttle plates, which have a vertical rotation axis, are placed. Both plates can be fixed at arbitrary rotations by means of a series of pins, that allow for complete port throttling control.

A structured plate meshing strategy was adopted to accomplish the plate modelling in the intake ducts, as reported in Figure 4. A simplified representation of the plates was introduced in the ports, by deactivating one layer of cells in either the streamwise or the crosswise direction, and rotating them up to the requested orientation angle. In this way, it was possible to maintain a block-structured, hexahedral mesh discretization that allows for accurate wall boundary treatment, at the price of a slight simplification in the plate shape.

In a detailed swirl modelling study [16] it was seen that this plate model is able to capture in-cylinder swirl trends well for a wide variety of plate orientations. Minor deviations from what was seen in the experiments occurred at plate angles between 50 and 70 degrees and led to underpredicted swirl by not more than about 20%. These are the conditions where the throttle model features maximum cell distortion.

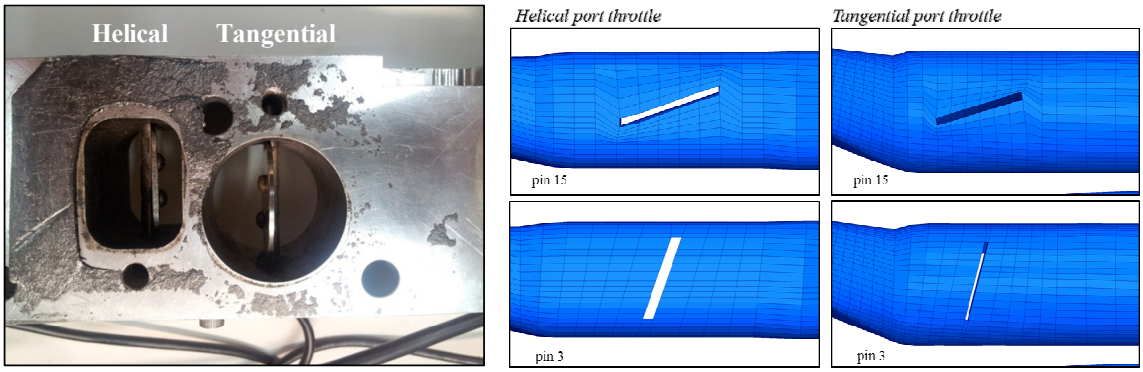


**Fig. 4.** Details of the swirl plates, and corresponding port mesh distortion strategy.

The in-cylinder flow structures at IVC for the four swirl ratios used in this study are reported in Figure 5. As the figure shows, the different swirl values obtained using different throttling strategies also lead to noticeably different in-cylinder flow structures.

The baseline configuration features Rs = 2.2, and both throttle plates are completely open. Here, the in-cylinder flow configuration is determined by port design, as significant swirling velocities are seen to enter the combustion chamber with a characteristic eddy length of the order of the intake valve diameter. At the same time, most of the large, cylinder-bore-scale momentum enters the combustion chamber from the tangential port, but with locally smaller velocity magnitudes at the crank angle shown.

Both configurations with higher swirl ratios were achieved by only throttling the helical port. This corresponded to having almost only one active intake port, thus changing engine breathing, but at the same time removing the smaller-scale intake swirl velocity components that partially oppose the large-scale flow entering from the tangential port. Both of these strategies are seen in Figure 5 to lead to significantly more solid-body-like vortex structures in-cylinder, and also significantly larger velocities within the bowl region, which may be relevant for increasing the efficiency of mixing in that region later in the cycle [9].

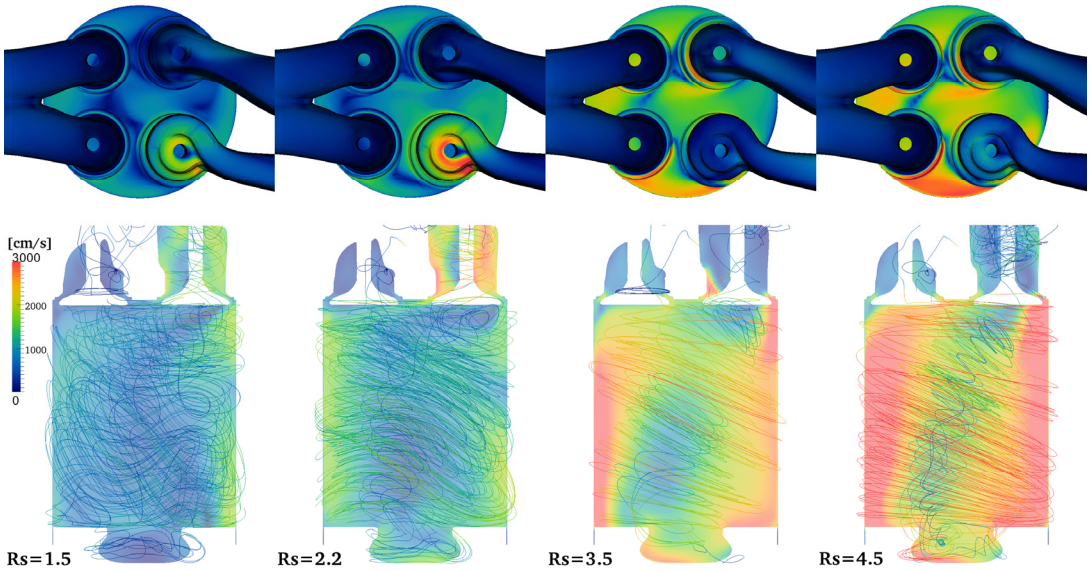


**Fig. 5.** Differences in predicted velocity field structures at BDC during the intake stroke. Velocity magnitudes (top) in the ports and near cylinder head; (bottom) at vertical planes intersecting the intake valves, also showing velocity streamlines.

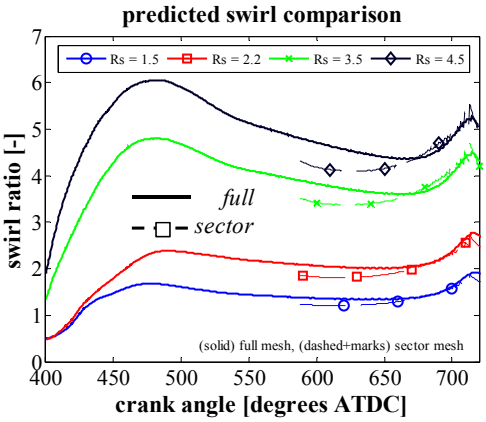


**Fig. 6.** Comparison between predicted in-cylinder swirl ratios with full (solid) and sector (dashed, marks) meshes

On the contrary, the lowest IVC swirl ratio was obtained by throttling both intake ports. The helical port was partially throttled by 20 degrees, and the tangential port throttled by 60 degrees [13]. The limited throttling of the helical port led to the significant swirl velocity components generating eddies at the intake valve scale. However, lack of significant large-scale flow entering from the tangential port led to a final vortex structure which is not very coherent and which still contains significant vertical velocity components.

In order to transfer the flow information into the sector mesh simulations, it was necessary to calibrate the IVC swirl profile with an 'effective' swirl ratio value. This was due to the fact that the axisymmetric mesh representation quickly destroys flow non-uniformities. Furthermore, azimuthal momentum conservation is enforced. Thus, the swirl ratio predicted with a sector mesh at the end of the compression stroke was observed to be significantly higher than the swirl ratio predicted with the full engine geometry, even when the same value was initialized at IVC. In order to have comparable results in terms of flow properties when injection occurs, the IVC swirl ratio value was calibrated at each swirl condition in order to match the near-TDC swirl ratios predicted by the full geometry calculation. This led to initializing the sector simulations at IVC with swirl ratios Rs = 1.236, 1.856, 3.502, 4.303, respectively.

## 4. Results

### 4.1 Flow study

The full geometry engine model was able to capture intake swirl ratios and near-TDC averaged tangential velocity profiles well, when compared to flow bench and PIV measurements [16]. However, the previous experiments had been used to provide suitable initialization data for sector mesh simulations, and did not provide sufficient insight into the development of the complex in-cylinder flow structures, and on the effects they have on fuel-air mixing.

Thus, current PIV experimental efforts [28,29] on the light-duty optical engine are focused on understanding the role of non-uniform, port- and piston-induced flow structures on fuel-air mixing and combustion development in the engine. Preliminary experimental data from the baseline Rs = 2.2 swirl configuration were used to assess the validity of the model, and to study the structure of the intake flow. It should be noted that in these experiments, the same swirl ratio as the baseline case [4] was achieved with a slightly different throttling strategy, that featured partial throttling of the helical port. The same configuration was used for the corresponding simulations.

Figures 7 to 9 summarize comparisons between predicted and measured velocities at three horizontal planes placed in the upper part of the combustion chamber, at distances dz = 10.0, 13.5, 17.0 mm from the fire-deck. The measurements were taken for a range of crank angles during the induction

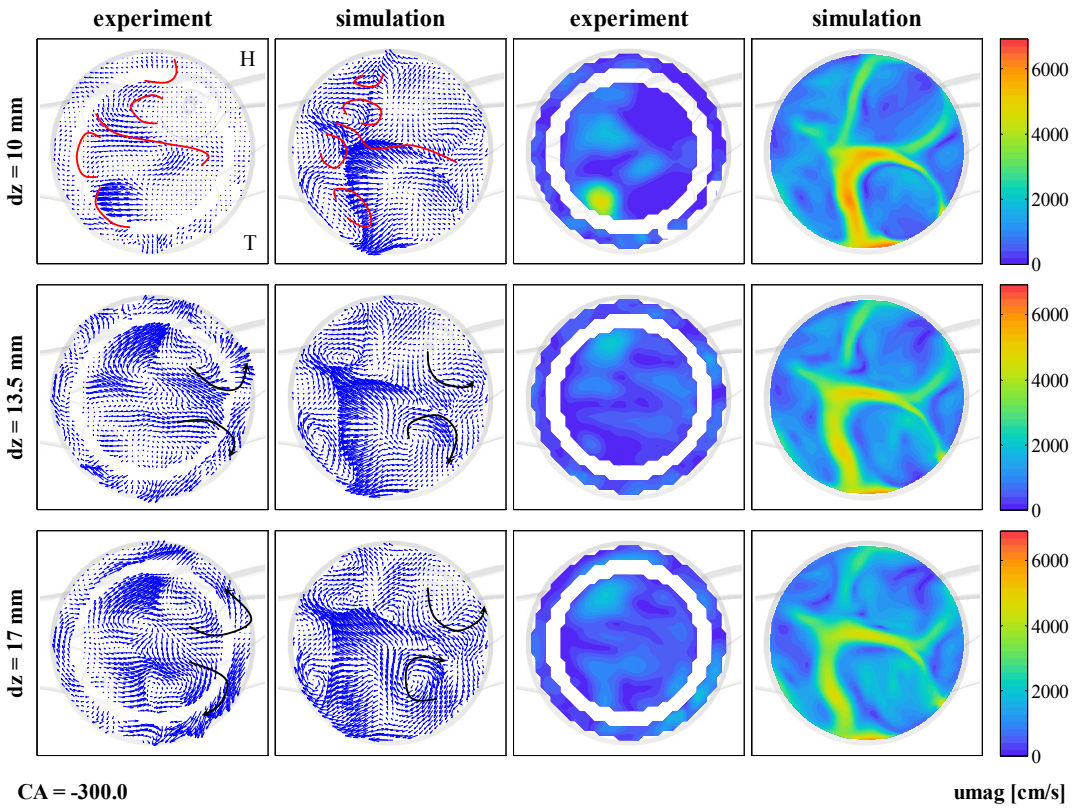


**Fig. 7.** Comparison between predicted and measured velocity vectors (left) and magnitudes (right, in cm/s) at the three PIV measurement planes, CA = 300 degrees bTDC.

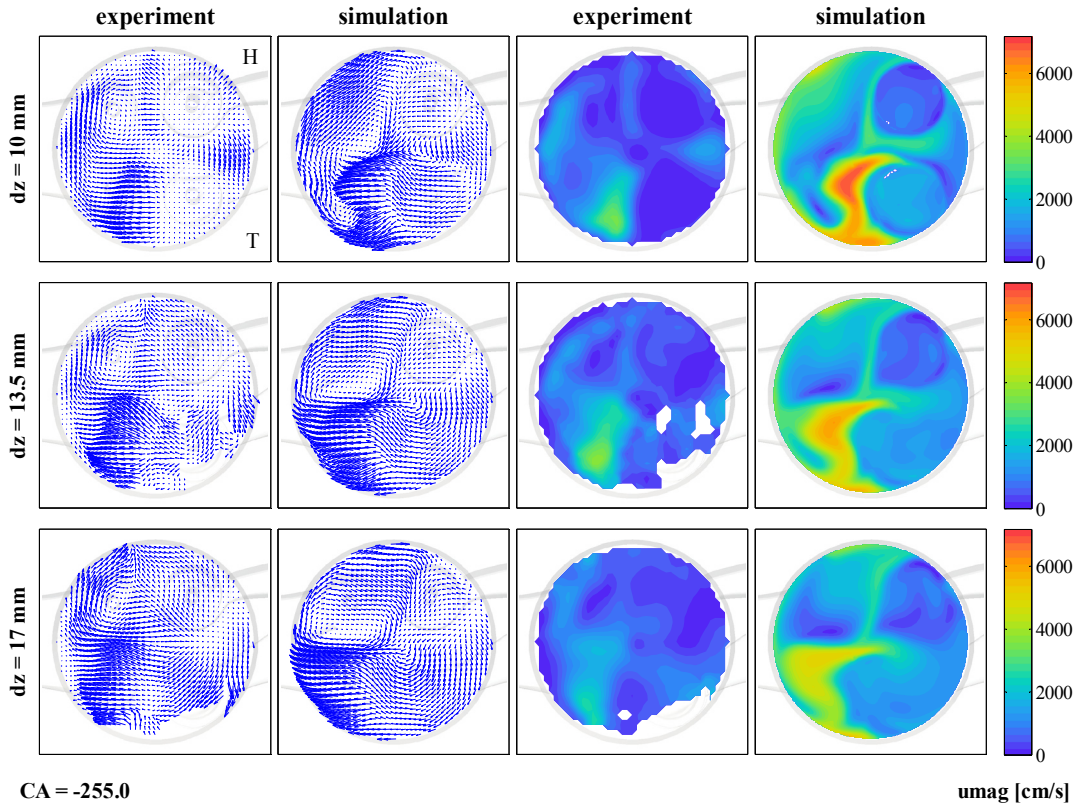


**Fig. 8.** Comparison between predicted and measured velocity vectors (left) and magnitudes (right, in cm/s) at the three PIV measurement planes near maximum valve lift, CA = 255 degrees bTDC

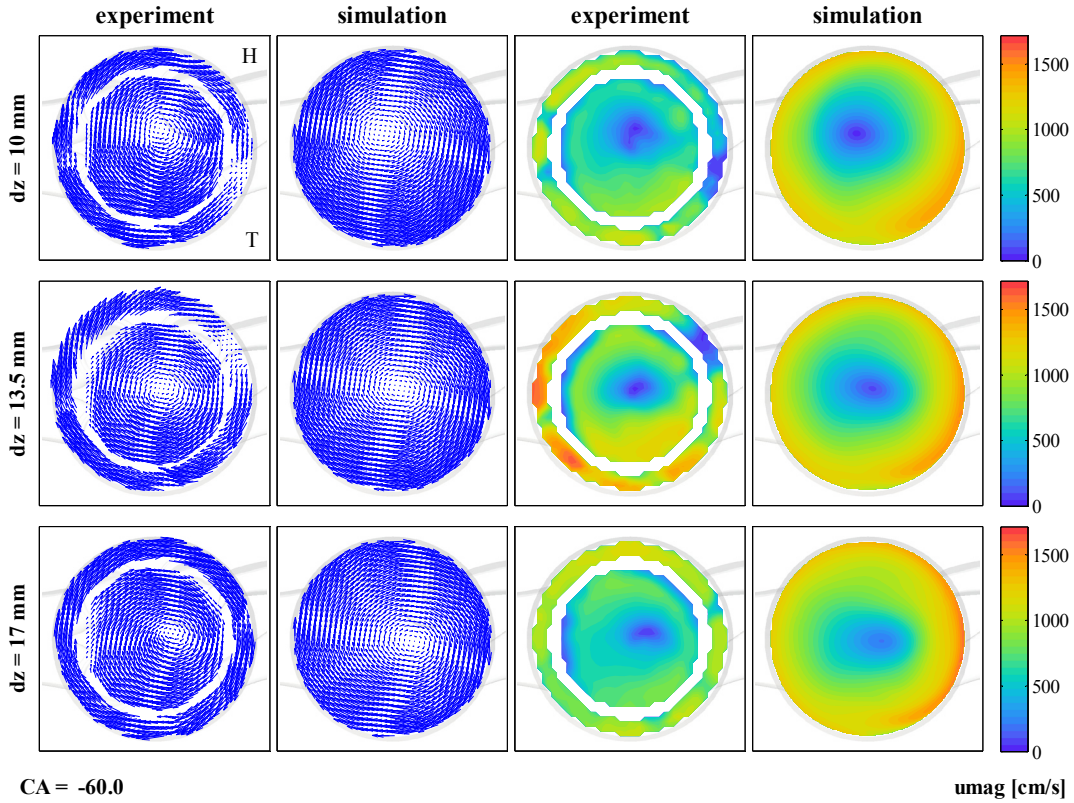


**Fig. 9.** Comparison between predicted and measured velocity vectors (left) and magnitudes (right, in cm/s) at the three PIV measurement planes after IVC, CA = 60 degrees bTDC

stroke, where the position of the optical piston, the intake valves and the laser sheet did not cause either loss of information or extreme signal noise. For the sake of brevity, we only show a few significant crank angles: CA = -300, -255, -60 degrees aTDC, which represent typical flow conditions after intake valve opening (IVO), near maximum intake valve lift, and after intake valve closure (IVC).

In the early intake flow of Figure 7, the simulation shows a 'momentum wall', displaced almost axially between the intake and the exhaust ports, due to the intake flow from either valve, which pushes towards the exhaust side, causing formation of four distinct vortex structures in the region below the exhaust valves (highlighted in red in the Figure). The same recirculation structures can be seen in the experiment too, even if more weakly defined, as stronger momentum from the tangential port is unbalancing the flow more towards the upper half of the plane. Interestingly, both the experiment and the simulation show that, as the horizontal section is moved downwards, it is possible to notice the formation of two counter-rotating vortices (highlighted in black in Figure 7) behind the wall formed by the intake flow, below the intake valves. These structures are formed by momentum transfer from the region with higher pressure, near the 'momentum wall', and the near-wall region behind the valves, following a mechanism which is evidently not much different than what happens around aircraft wings.

When approaching maximum valve lift, as in Figure 8, the intake flow is more developed and it is possible to recognize clearer similarities between the experimental measurements and the simulation, both in flow structure and in velocity magnitudes. First, the formation of stronger velocity components at the outlet of the tangential intake valve (lower-right corner) fosters the generation of a cylinder-bore-scale large eddy, which has already traveled for almost half of the circumferential extent of the cylinder bore, as witnessed by the large tangential velocity components present near the liner in the second, upper-left quadrant of the plane. Both measurement and simulation also show how the flow entering through the helical port, which has a well-defined eddy size of the order of the valve diameter, is also getting deviated into the main-stream large-scale eddy within these planes. This leads to the formation of a stagnation region below the upper left exhaust port.

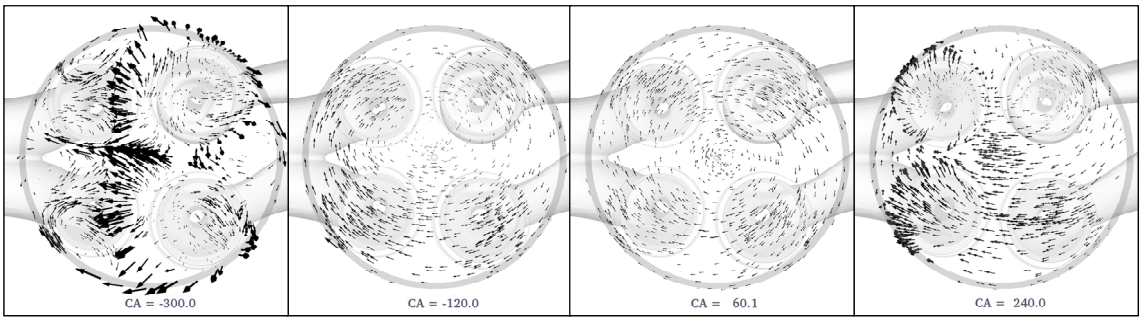


**Fig. 10.** Distinct flow regimes during the cycle. Crank angles (left to right): -300, -120, +60, +240 aTDC

After IVC, as shown in Figure 9, no intake flow is occurring, and the velocity field structure within the combustion chamber gradually rearranges itself into a unique, large-scale vortex, whose swirl center is not axial with the cylinder but has a precessive movement and a vertical tilt, which ultimately reflects the flow non-uniformity.

Four different regimes were seen as the major flow structure types occurring during the engine cycle. These regimes are summarized in Figure 10. The first one represents flow during intake. Intake velocities enter the combustion chamber with strong vertical components, and the momentum ratio between the tangential and the helical port is mostly determined by the throttling strategy. Whatever the ratio, both ports contribute to the formation of a definite 'momentum wall' which initially splits the combustion chamber in half – the part below the exhaust valves is pushed towards the liner, and thus recirculation regions form. The part below the intake valves sees the formation of two eddies having the size of the valves, set into motion by the pressure difference introduced by the intake flow.

The second flow regime in the engine starts to form close to IVC, when a cylinder-bore-scale vortex forms and gradually absorbs all of the residual non-vortex structures. As a result, the vortex center tilts within the combustion chamber, and exhibits a precessing movement.

The third flow regime is established after TDC, during the expansion stroke. In this case where no spray events occur, most of the momentum non-uniformities have dissipated, and the flow now shows an axisymmetrical vortex structure.

Finally, when the exhaust valves open, and flow starts entering the exhaust ports, residual swirling velocity components are small. Thus, an almost uniflow scavenging is established, with the main motion direction from the intake to the exhaust valve region.

### 4.2 Mixture preparation study

The code was used to study mixture preparation in the presence of a single-pulse injection, typical of a Partially Premixed Combustion (PPC) strategy, at all four swirl ratios. The operating condition represented a 1500 revs/min, slightly boosted, low-load case, with 3 bar indicated mean effective pressure (IMEP), and an EGR ratio of 55%. The injection profile for the 8.8 mg fuel was measured experimentally [5] for the same PRF fuel blend used in the engine experiments. The mixture preparation experiments were run using a non-reacting, pure nitrogen gas composition, and showed that most of residual engine-out unburned hydrocarbon (UHC) and carbon monoxide (CO) emissions which occur in the combusting cases are due to overly-lean mixtures forming, especially in the squish region and in the central, upper part of the combustion chamber, and not undergoing complete oxidation. Figures 11 to 16 compare the sector simulation results with the mixture preparation experiments [20,24].

In the squish plane (P1), as reported in Figures 11-13, the simulations reveal two distinct phenomena affecting the vapor jet development. In the central part of the cylinder, the jet is twisted by the swirling velocities into a hook-like structure, which is more significant the stronger the swirl ratio. This structure evolves throughout the cycle. Early after the end of injection (Figure 11) it still appears to be

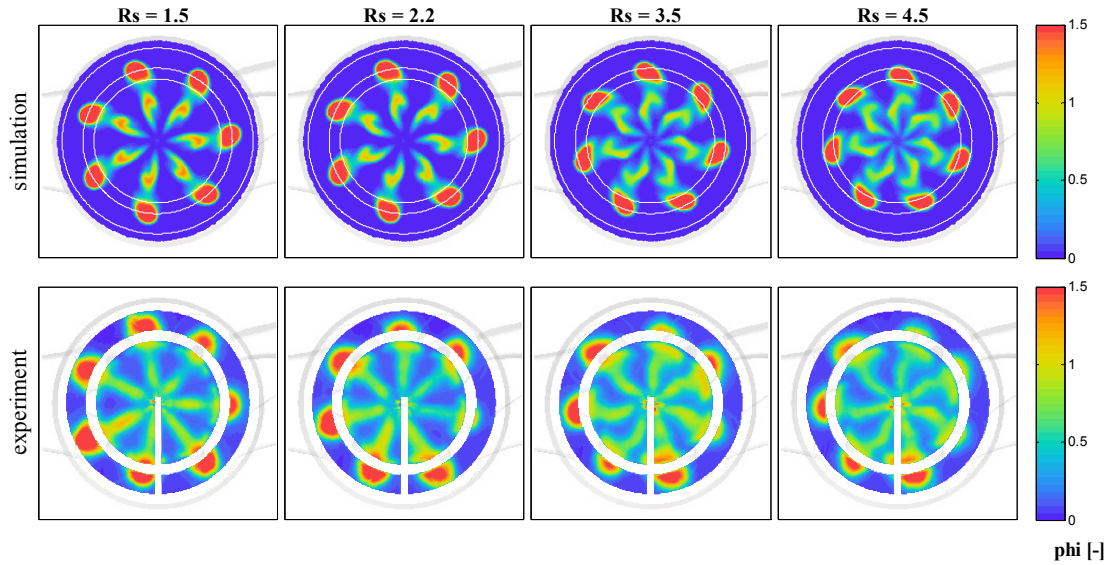


**Fig. 11.** Squish plane (P1) PRF25 mixture preparation comparison. Swirl ratios: 1.5, 2.2, 3.5, 4.5; CA = -15.0.

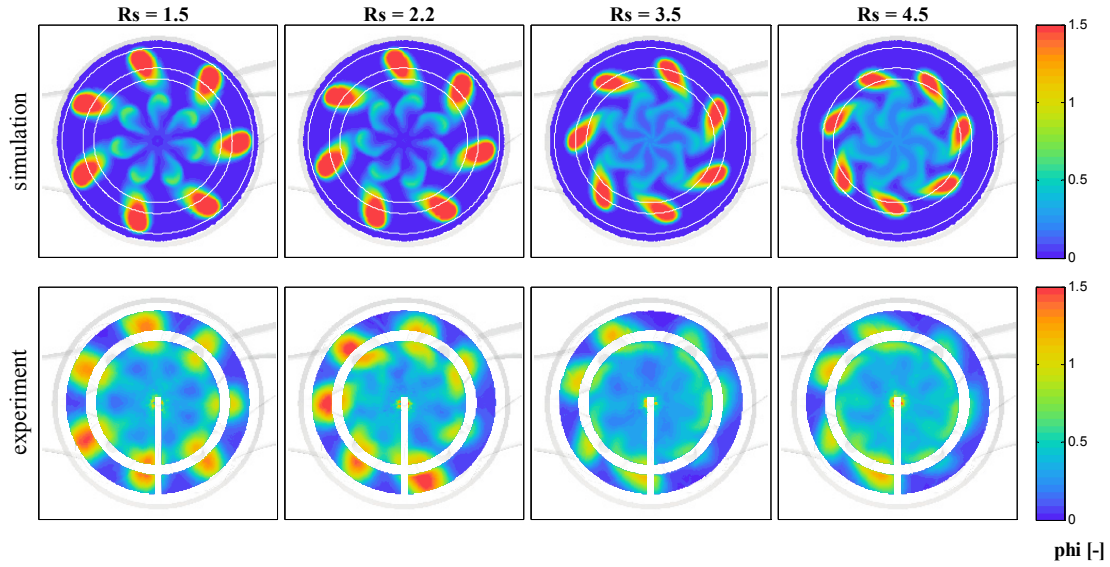


**Fig. 12.** Squish plane (P1) PRF25 mixture preparation comparison. Swirl ratios: 1.5, 2.2, 3.5, 4.5; CA = -10.0.

definite, and quite self-contained. Later, after the end of injection (Figure 13), immediately before high temperature heat release takes place, the jets are completely mixed to an almost homogeneous, lean ($\phi$ < 0.5) equivalence ratio. The simulations show a slight under-prediction of the mixing phenomenon in the lowest swirl cases, where turbulent diffusion is a more significant part of the mixing process, suggesting the sector approach's inability to capture the in-cylinder turbulence levels.

Jet penetration into the squish region is also crucial to pollutant formation. In Figure 11 the model shows an over-dependency of jet tip penetration on swirl ratio compared to that seen in the experiments. The penetration is well captured at Rs = 1.5 and 2.2, while it is quite underestimated at the highest swirl ratios. However, both the simulations and the experiments indicate a clear reduction in penetration with higher flow swirl.

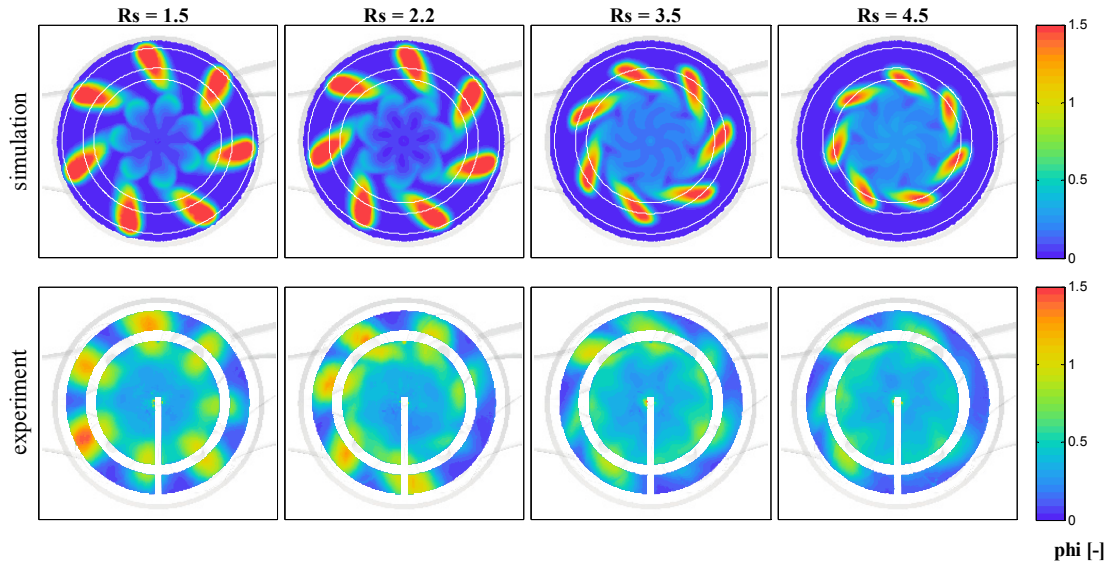


**Fig. 13.** Squish plane (P1) PRF25 mixture preparation comparison. Swirl ratios: 1.5, 2.2, 3.5, 4.5; CA = -5.0.

Mixture preparation at the bowl rim (plane P2) is linked to penetration into plane P1, especially as far as targeting of the fuel jet against the rim is concerned. The simulation shows significant impingement against the rim already at -15 degrees aTDC (Figure 14). This phenomenon is not seen in the experimental images due to the limited extent of the measurement that cannot reach the bowl rim wall due to interference from bowl rim reflections. Here most of the jet-to-jet differences are seen, not only in the peak equivalence ratio, but also in its shape and thickness. It should be also noted that the experimental image also retains some details, including the nozzle exits, which are part of the background and are not intersected by this plane.

Closer to the high temperature heat release phase, in Figure 15, the simulations still show quite well defined jet structures, which are much more blurred in the experimental images. This is again consistent with the underprediction of turbulent diffusion by the model; however, good agreement in terms of the average in-plane equivalence ratios is seen.

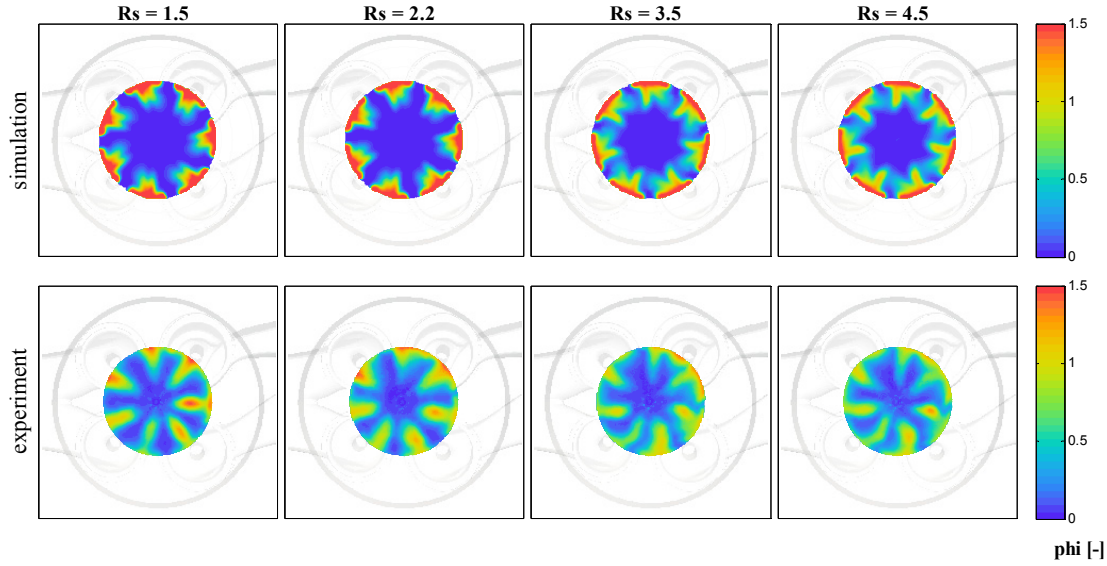


**Fig. 14.** Bowl rim plane (P2) PRF25 mixture preparation comparison. Swirl ratios: 1.5, 2.2, 3.5, 4.5; CA = -15.0.

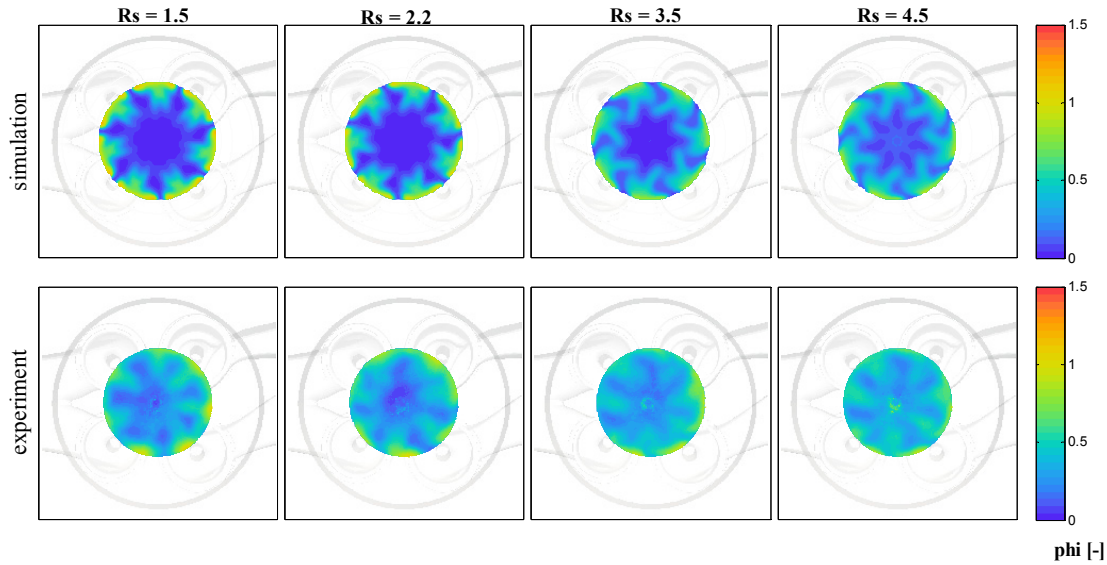


**Fig. 15.** Bowl rim plane (P2) PRF25 mixture preparation comparison. Swirl ratios: 1.5, 2.2, 3.5, 4.5; CA = -10.0.

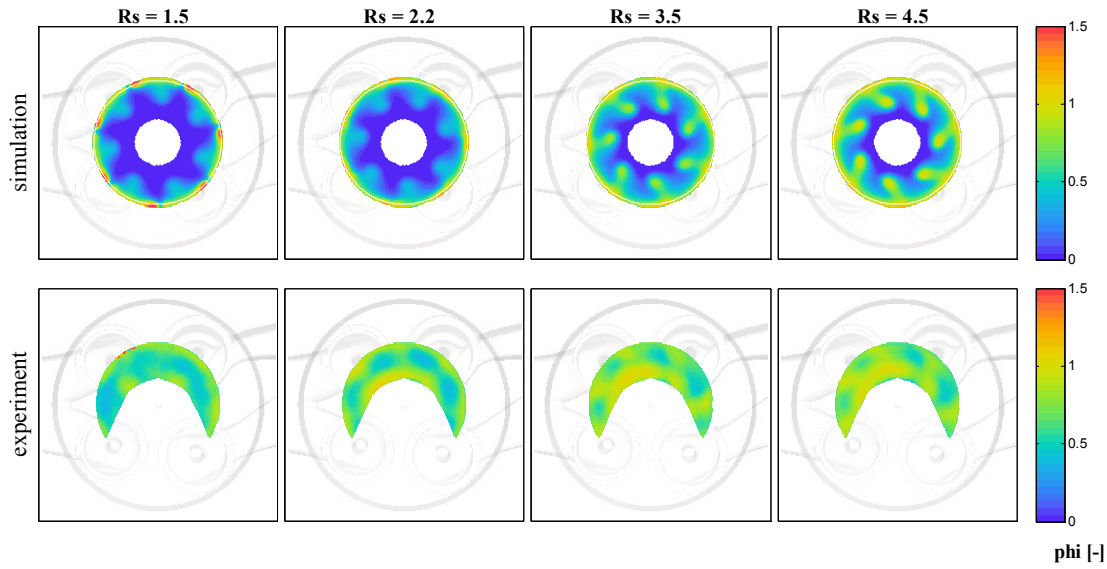


**Fig. 16.** Bowl plane (P3) PRF25 mixture preparation comparison. Swirl ratios: 1.5, 2.2, 3.5, 4.5; CA = -5.0.

Finally, penetration deep into the bowl, crossing plane P3 (Figure 16), and re-appearing towards the center of the combustion chamber after having travelled along floor of the bowl, is both an indicator of how well jet penetration is captured, and of how well the mixing has been predicted. Simulations at all swirl ratios were able to capture the jet tip penetration re-entering plane P3, but at a larger radius than seen in the experiments, i.e., farther from the cylinder center. This suggests that the angular momentum in the head of the jet is greater in the simulation than is seen experimentally. It is this angular momentum, causing the jet to spin out toward the bowl periphery, that inhibits the jet from following the bowl contour. At the same time, mixing appears to have been again slightly underestimated. In the experiments the jet structures can still be identified, but the average equivalence ratios were quite well captured.

## Summary and Conclusions

A computational model of the Sandia National Laboratories light-duty optical access engine was built using an unstructured version of the KIVA code for which a comprehensive set of spray models has been implemented. Two grids, one representing one seventh axisymmetric sector of the combustion chamber, and a full engine grid including the intake and exhaust ports, vessels, and the swirl generation plates in the optical engine, were used to test the model performance at predicting flow and mixture preparation.

The following conclusions were derived from this study:

- Sector mesh models are quite effective in providing a reasonable estimate of the in-cylinder spray structure and mixture preparation. However, they cannot explain the effects that local geometric features have on the fuel-air mixing process. They also cannot properly resolve the turbulence flow field, which, even with well resolved meshes, results in a lack of mixing due to underpredicted turbulent diffusion.

- The present full geometry flow structure study suggests that the engine's port design, usually tailored for conventional diesel combustion strategies, may be relevant for the optimization of engines running lean and low-temperature combustion strategies, where an excess of mixing can lead to the formation of lean mixture pockets that can misfire, causing high unburned hydrocarbon and carbon monoxide emissions.

- The present spray simulations demonstrated the overall reliability of spray models with axisymmetric, equally spaced grids, but still need further validation with arbitrary grids, including non-polar displaced, skewed or unstructured cells.

The study suggests that proper engine design for advanced combustion strategies still requires research in improving the understanding and suitably modeling both spray and turbulence properties. However, flow details seen with the RANS simulation framework appear to be suitable for engineering design applications.

## Acknowledgements

This work was performed at the University of Wisconsin-Madison Engine Research Center and at the Combustion Research Facility of Sandia National Laboratories in Livermore, California. Support for this research was provided by the U.S. Department of Energy, Office of Vehicle Technologies. Sandia is a multi-program laboratory operated by Sandia Corporation, a Lockheed Martin Company, for the United States Department of Energy's National Nuclear Security Administration under contract DE-AC04-94AL85000.

The authors would also like to acknowledge ANSYS inc. for granting ICEM CFD licenses for mesh generation to the Engine Research Center.

## References

1. Abani N, Munnannur A, Reitz RD, "Reduction of Numerical Parameter Dependencies in Diesel Spray Models", Journal of Engineering for Gas Turbunes and Power 130, 032809, 2008.
2. Bailey AB, Hiatt J, "Sphere Drag Coefficients for a Broad Range of Mach and Reynolds Numbers", AIAA Journal 10(11), 1436-1440, 1972.
3. Beale JC, Reitz RD, "Modeling Spray Atomization with the Kelvin-Helmholtz/Rayleigh-Taylor hybrid model", Atomization and Sprays 9, 623-650, 1999.
4. Bergin M, Reitz RD, "Effect of Flowfield Non-Uniformities on Emissions Predictions in HSDI Engines", SAE technical paper 2011-01-0821, 2011.
5. Busch S (2014) personal communication.
6. Colban WF, Kim D, Miles PC, Oh S, Opat R, Krieger R, Foster D, Durrett R, Gonzalez MA, "A Detailed Comparison of Emissions and Combustion Performance Between Optical and Metal Single-Cylinder Diesel Engines at Low Temperature Combustion Conditions", SAE technical paper 2008-01-1066, 2008.

7. Dempsey A, Wang B, Reitz RD, Petersen B, Sahoo D, Miles PC, “Comparison of Quantitative Equivalence Ratio Measurements with CFD Predictions for a Light-Duty Low Temperature Combustion Diesel Engine”, SAE Int. J. Engines 5(2):2012, doi:10.4271/2012-01-0143.
8. Ekoto IW, Colban WF, Miles PC, Park SW, Foster DE, Reitz RD, Aronsson U, Andersson, O, “UHC and Co emissions Sources from a Light-Duty Diesel Engine Undergoing Dilution-Controlled Low-Temperature Combustion”, SAE technical paper 2009-24-0043, 2009, doi:10.4271/2009-24-0043.
9. Ge H-W, Reitz RD, Willelms W, “Modeling the effects of In-Cylinder Flows on HSDI Diesel Engine Performance and Emissions”, SAE Int. J. Fuels Lubr. 1, 293-311, 2008. Doi:10.4271/2008-01-0649.
10. Han Z, Reitz RD, “Turbulence Modeling of Internal Combustion Engines Using RNG k-epsilon Models”, Combustion Science and Technology 106, 267-295, 1995.
11. Morrison FA, “Data Correlation for Drag Coefficient for Sphere”, Department of Chemical Engineering, Michigan Technological University, 2013.
12. Munnannur A, Reitz RD, “Comprehensive collision model for multidimensional engine spray computations”, Atomization and Sprays 19(7), 597-619, 2009.
13. Opat RM, “Investigation of mixing and temperature effects on UHC/CO emissions for highly dilute low temperature combustion in a light-duty Diesel engine, M.Sc. Thesis, University of Wisconsin-Madison, 2006.
14. Perini F, Dempsey A, Sahoo D, Miles PC, Reitz RD, “A computational investigation of the effects of swirl ratio and injection pressure on wall heat transfer in a light-duty diesel engine”, SAE technical paper 2013-01-1105, 2013.
15. Perini F, Galligani E, Reitz RD, “An analytical Jacobian approach to sparse reaction kinetics for computationally efficient combustion modelling with large reaction mechanisms”, Energy and Fuels 26(8), 4804-4822, 2012.
16. Perini F, Miles PC, Reitz RD, “A comprehensive modeling study of in-cylinder fluid flows in a high-swirl, light-duty optical diesel engine”, Computers and Fluids, submitted, 2013.
17. Perini F, Sahoo D, Miles PC, Reitz RD, “Modeling the ignitability of a pilot injection for a Diesel Primary Reference Fuel: impact of injection pressure, ambient temperature and injected mass”, SAE technical paper 2014-01-1258, 2014.
18. Petersen BR, Ekoto IW, Miles PC, “An Investigation into the Effects of Fuel Properties and Engine Load on UHC and CO Emissions from a Light-Duty Optical Diesel Engine Operating in a Parttially Premixerd Combustion Regime”, SAE Int. J. Engines 3 (2010), 38-55. Doi:10.4271/2010-01-1470
19. Petersen BR, Miles PC, “PIV Measurements in the Swirl-Plane of a Motored Light-Duty Diesel Engine”, SAE Int. J. Engines 4(1), 1623-1641, 2011.
20. Petersen BR, Sahoo D, Miles PC, “Review of Equivalence Ratio Measurements in a Light-Duty Diesel Engine Operating in a Lioght-Load Partially Premixed Regime”, THIESEL 2012 Conference on Thermo- and Fluid Dymanic Processes in Direct Injection Engines.
21. Ra Y, Reitz RD, “A reduced chemical kinetic model for IC engine combustion simulations with primary reference fuels”, Combustion and Flame 155(4), 713-738, 2008.
22. Reitz RD, “Directions in Internal combustion engine research”, Combustion and Flame 160(1), 1-8, 2013.
23. Sahoo D, Miles PC, Trost J, Leipertz A, “The Impact of Fuel Mass, Injection Pressure, Ambient Temperature, and Swirl Ratio on the Mixture Preparation of a Pilot Injection”, SAE Int. J. Engines 6(3):2013, doi:10.4271/2013-24-0061.
24. Sahoo D, Petersen B, Miles PC, “Measurement of Equivalence Ratio in a Light-Duty Low Temperature Combustion Diesel Engine by Planar Laser Induced Fluorescence of a Fuel Tracer”, SAE Int. J. Engines 4(2):2011,2312-2325, doi:10.4271/2011-24-0064.
25. Torres DJ, Trujillo MF, “KIVA-4: An unstructured ALE code for compressible gas flow with sprays”, Journal of Computational Physics 219(2), 943-975, 2006.
26. Torres DJ, O’Rourke PJ, Amsden AA, “A discrete multicomponent fuel model”, Atomization and Sprays 13(2-3), 1-42, 2003.
27. Wang Y, Ge H-W, Reitz RD, “Validation of Mesh- and Timestep-Independent Spray Models for Multi-Dimensional Engine CFD Simulation”, SAE Int. J. Fuels Lubr. 3(1), 277-302, 2010.
28. Zha K (2014) personal communication.
29. Zha K, Busch S, Miles PC, “Progress Towards In-Cylinder PIV Measurements throughout the Full Intake and Compression Strokes”, Sandia National Laboratories technical report SAND 2014-3118P, 2014.